Table of Contents

Uncertainty Analysis for manoeuvring predictions based on captive manoeuvring tests

1. PURPOSE OF PROCEDURE

The purpose of the procedure is to provide an example for the uncertainty analysis (UA) of a model scale towing tank planar motion mechanism (PMM) test following the ITTC Procedures 7.5-02-01-01 Rev 00, 'Uncertainty Analysis in EFD, Uncertainty Assessment Methodology' and 7.5-02-01-02 Rev 00, 'Uncertainty Analysis in EFD, Guidelines for Towing Tank Tests.'

This procedure starts with listing a extensive list of sources of uncertainties. Although exhaustive, this list is not complete and may need to be augmented based on the model basin, model set-up, and measuring equipment of every individual model test institute.

The example in appendix A is based on the IIHR results of a research carried out before 2008. This example addresses many of the sources of the uncertainty, but not all of them. Furthermore, the worked out example in Appendix A, only addresses the uncertainties of the measured forces and moments, and does not address yet the elaboration into the uncertainty on hydrodynamic coefficients and the uncertainty of the predicted manoeuvres.

2. SOURCES OF UNCERTAINTY

During captive manoeuvring tests, a ship model is forced by an external mechanism to undergo a prescribed trajectory in the horizontal plane. The measurement of forces acting of the model leads to the numerical value of a number of characteristic coefficients occurring in the mathematical manoeuvring model, which can be used for predicting various aspects of manoeuvring behaviour, including standard manoeuvres such as turning circle tests and zigzag tests.

The accuracy of test results is influenced by imperfections of the experimental technique.

This relates to anything which is measured, including position, velocity and accelerations (translations and rotations) and obviously the forces and moments. The sources of uncertainties are grouped in different origins: uncertainties in the planar motion mechanism; the set-up in the basin, .

2.1 Inaccuracy of ship model characteristics;

The influence of some factors (e.g. uncertainties on main dimensions, offsets, loading condition) on the accuracy of test results is hard to estimate, while variations of other parameters (e.g. mass, moments of inertia) have a rather straightforward effect on the forces acting on the model.

- Length
- Uncertainty in the individual masses
- Uncertainty in the placement of the individual masses (because this determines x_G and the radii of inertia)
- The draught mark as drawn on the model
- Loading of the model to the draught mark

- Rudder and propeller manufacturing accuracy
- Model alignment
- Drift angle setting
- Rudder alignment
- Rudder angle setting
- Propeller rate setting for the tests.
- Water density (as a function of water temperature)
- Propeller rate measurement

2.2 Planar Motion Mechanism geometry discrepancies.

The geometry of the planar motion mechanism and, therefore, the trajectory of the ship model may be influenced by elastic deformation, backlash and mechanical imperfections, causing geometrical uncertainties which may affect model kinematics and dynamics.

A detailed analysis highly depends on the type and concept of the mechanism. Following factors may be of importance in the case of a PMM system with three degrees of freedom:

- deviations of the main carriage with respect to the tank:
  - horizontal deviations of the main carriage's guiding rail;
  - backlash between guiding rail and horizontal guiding wheels;
  - accuracy of the guiding wheels (radius, eccentricity, backlash);
  - vertical deviations of both rails;
  - accuracy of the main carriage's wheels (radius, eccentricity, backlash);

- deviations of the lateral carriage with respect to the main carriage :
  - alignment of guiding for lateral carriage;
  - perpendicularity of guiding for lateral carriage with respect to main carriage;
  - backlash of guiding for lateral carriage;

- deviations of the rotation table with respect to the lateral carriage :
  - alignment of rotation axis;
  - verticality of guiding for yaw table;
  - backlash;

- deviations of the model connection system with respect to the rotation table;

- inaccuracies of the connection of the ship model to the mechanism.

With respect to the latter, a distinction should be made between connection inaccuracies according to either the free or the forced motion modes. Captive model tests executed for investigation of manoeuvring of surface ships require forced surge, sway and yaw motions, while the model is usually free to heave and pitch. Roll motions may be free or forced.

Some uncertainties are caused by imperfections of the connection system:

- geometry imperfections and backlash may cause position uncertainties in all motion modes;
- mechanical friction between moving parts may result into position uncertainties in the free motion modes;
- inaccurate mounting may induce position uncertainties in all forced motions modes;

but even a perfectly functioning connection may induce position uncertainties in the forced modes due to motions in the free modes. Due to the concept of some connection systems, pitch and heave indeed induce a small surge component.

2.3 Planar Motion Mechanism control and setting uncertainties

The kinematics of the driving mechanism and, therefore, of the model are determined by a number of directly controllable parameters s_i which are either kept constant or controlled according to a time function during a test run. Setting and control uncertainties on these parameters indirectly influence the forces acting on the model. An analysis of this influence strongly depends on the concept of the mechanism and the type of test.

Divergences between prescribed and actual trajectories can also be caused by inaccuracy of the measurement of position or speed of the (sub-)mechanisms, affecting the control system's feedback signal. Possible causes are:

- temperature influence;
- slip (of encoder wheel), backlash;
- uncertainties/deformation in transmission to encoder;
- resolution of encoder.

Special attention should be paid to possible limitations of the mechanism concept, which may not allow the execution of some from theoretical point of view desirable trajectories. For example, small amplitude PMM systems based on the combined action of two horizontal oscillators may not be able to perform a pure harmonic yaw motion. In other cases, limitations of the control system yield deviations from the theoretically desired trajectory: this is for instance the case if a PMM system is mounted on a towing carriage which is not equipped with a variable speed control, as this leads to fluctuations of the ship's forward speed component during a harmonic yaw test. Principally, such discrepancies are predictable and can be accounted for during analysis. The uncertainty in the PMM amplitude(s) (position or velocity) can be estimated from the standard deviation of the dataset to a Fourier fit through the data set.

2.4 Uncertainties on ship control equipment parameters

During a test run, a number of control equipment parameters (propeller rpm, rudder angle, ...) are controlled; setting or control uncertainties have a direct influence on the forces acting on the model.

2.5 Measurement accuracy

The quality of force measurements may be affected by non-linearity, hysteresis, sensitivity, accuracy of calibration, ... Uncertainties on position and speed measurements not only affect the mechanism's control loop (see above), but also the interpretation of the measured forces.

2.6 Undesired facility related hydrodynamic effects

A ship model's dynamics and, therefore, test results may be affected by several influences caused by the limitations of the experimental facility, so that tests are not performed in unrestricted still water. Some examples:

- Residual motion of the water in the tank may affect the model's dynamics if the waiting time between two runs is too short.
- Non-stationary phenomena occurring during transition between acceleration and steady phases or if harmonical techniques are applied may also affect the model's dynamics.
- Tank width and also length limitations induce undesired additional forces.
- In shallow water tests, bottom profile variations affect the model's dynamics.

The influence of these effects on the accuracy of test results generally increases with decreasing water depth. Although complete prevention is principally impossible, the effects can be reduced by an adequate selection of test and analysis parameters.

2.7 Data acquisition

Deformation of the measured signals may be induced by signal processing techniques, due to characteristics of e.g. filters, AD-conversion (resolution, time step).

2.8 Post-model test numerical analysis

Post model tests, the time traces will be processed to obtain the average of signals or the in- and out-phase of signals. As part of this, uncertainties will be introduced or removed.

(Possible) filtering of the time traces of the measured forces and moments (and velocities). Appropriate filtering should be applied, but care should be made not to filter too much, because in that case, essential information will be deleted. It is mentioned that a Fourier-fit of a signal obtained in an oscillation test is a filter.

- Obtaining the average of a CMT or drift tests, or the Fourier series of a oscillation test. The uncertainty for the data set about the fitted Fourier curve used in the PMM analysis should be included. The higher the order of the Fourier transform fitted to the data, the more flexible the curve. Thus small changes in the individual force measurements (within the calibration uncertainty of the force gauges) can result in large changes in the output derivatives. The sensitivity of the obtained derivative should be obtained by a suitable method (with Monte Carlo type approach being appropriate). An example is given by Woodward (2013), this paper is discussed in the ITTC manoeuvring committee report of the 27th ITTC conference.
- Uncertainties in the correction for the force and moment for the rotational velocity (centrifugal force) will need to be addressed.
- Fitting of all the results of all tests will also result in an uncertainty, which will be called a data-fitting uncertainty. This will depend on the selected mathematical model that will be used for the simulations.

The accuracy of calculated average values and harmonics appears to depend on test parameters (e.g. integration length, test frequency, number of cycles).

3. UNCERTAINTY OF THE PREDICTIONS

The total uncertainty of the manoeuvring predictions based on the measured forces and moments during captive model tests, is the result of a set of Monte Carlo simulations. A procedure using the following steps is recommended.

- Derivation the uncertainty of forces and moments for drift angles, rate of turn, rudder angles, and combinations of these settings. This part is elaborated in the example described in the appendix A.
- Based the uncertainty of every measured force and moment, using the Monte Carlo approach, multiple fits can be made. Every fit is a unique combination of hydrodynamic coefficients corresponding to a selected mathematical model. An example is elaborated by Woodward (2013).
- Using fast time domain simulations of each of these multiple fits, simulate time traces of trajectories of standard manoeuvres, such as turning circle manoeuvres

and zigzag manoeuvres, and possibly other objective manoeuvres that are of interest.

- Analyse the time traces to obtain key parameters such as overshoot angles obtained from zigzag tests or tactical diameters obtained from turning circle tests. This will hence result in a distribution of tactical diameters and overshoot angles. From this distribution, determine the uncertainty of the key parameters such as overshoot angles and tactical diameters.

4. REFERENCES

Benedetti, L., Bouscasse, B., Broglia, R., Fabbri, L., La Gala, F., and Lugni, C., 2006, "PMM Model Test with DDG51 Including Uncertainty Assessment," INSEAN Report No. 14, 174 pp.

Simonsen, C., 2004, "PMM Model Test with DDG51 Including Uncertainty Assessment," Force Technology Report No. ONRII187 01, 145 pp.

Woodward, M. D. 2013, Propagation of experimental uncertainty from force measurements into manoeuvring derivatives. AMT conference, Poland, 2013.

Yoon, H.-S., Longo, J., Toda, Y., and Stern, F., 2008, "PMM Tests and Uncertainty Assessment for Surface Combatant Including Comparisons Between Facilities," IIHR – Hydroscience & Engineering Report

Appendix A.

Example of uncertainty of measured force during PMM captive drift test and oscillation test

The Present example is developed in collaboration between IIHR-Hydro science & Engineering (IIHR), Force Technology, Instituto Nazionale per Studi ed Esperienze di Architettura Navale (INSEAN), and the 24th – 25th ITTC Manoeuvring Committee, including overlapping tests using the same model geometry for comparison of results and identification of facility biases and scale effects. Details of the UA procedures are provided by Simonsen (2004), Benedetti et al. (2006), and Yoon et al. (2007), including in the latter case comparisons between facilities and analysis of facility biases, scale effects, and parameter trends. Since at the time of writing this example, the state-of-the-art was not ISO GUM, many of the wordings in the example are related to bias and precision limits, instead of the later preferred type A and type B uncertainties.

This example provides an uncertainty assessment for a model scale towing tank PMM test for an un-appended model ship except bilge keels (i.e. without shafts, struts, propellers, and rudders) which is mounted free to heave and pitch, but fixed in roll. The PMM test conforms to the ITTC Procedures 7.5-02-06-02 Rev02, 'Captive Model Test Procedure.' Uncertainties for multiple runs are estimated for the non-dimensional forces and moment in model scale for four types of PMM tests (static drift, pure yaw, pure sway, and yaw and drift) at one Froude number (Fr = 0.280). Other PMM tests, such as static rudder, static drift and rudder, static drift and heel, dynamic yaw and rudder, dynamic yaw and drift and rudder, are not considered. This example does not provide UA for hydrodynamic derivatives derived from the forces and moment data or their effect on the full scale manoeuvring simulations. Additionally, UA estimates for heave and pitch are not provided.

The effect of data conditioning such as filtering or fairing, for example, Fourier Series reconstructions for the measured forces /moment and motions is not counted in this UA procedure. This procedure assumes that the measured forces/moment is the sum of those from all forces/moment gauges used for the case of multiple gauge system, and that the inertia forces/moment from parts for model installation are subtracted from the total measured forces and moments if the parts are suspended from the load cells. This procedure also assumes that the model ship is free to heave and pitch, and fixed in roll. The effect of deviations from the upright position such as roll or heel angle is not considered in this procedure. Finally, carriage speed is assumed to be constant, so the effect of acceleration caused by fluctuating carriage speed during runs is not considered.

1. Test Design

The tests are conducted in the IIHR towing tank, which is 100m long, 3.048m wide and 3.048m deep, and equipped with a drive carriage, PMM carriage, automated wave dampener system, and wave-dampening beach. A right-handed Cartesian coordinate system is fixed to the model. The origin is at the intersection of the mid-ship plane, centre plane, and water plane. The x, y, z axes are directed upstream, transversely to starboard, and downward, respectively (See Figure 1).

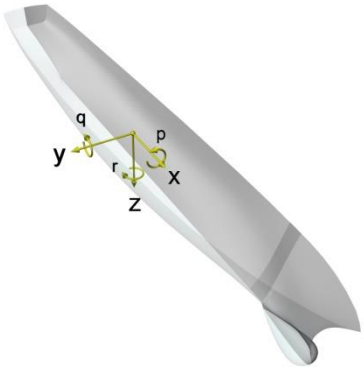

Figure 1 Coordinate system.

The model geometry is DTMB model 5512, a 1:46.6 scale, L_{PP} = 3.048 m. The model is unappended except for port and starboard bilge keels, i.e., not equipped with shafts, struts, propulsors, or rudders. To initiate transition to turbulent flow, a row of cylindrical studs of 1.6 mm height and 3.2 mm diameter are fixed with 9.5 mm spacing at x/L_{PP} = 0.45. The stud dimensions and placement on the model are in accordance with the recommendations by the 23rd ITTC (ITTC, 2002). Model- and full-scale geometric parameters for 5512 are summarized in Table 1.

		Ship	Model
λ	-	1 : 1	1 : 46.588
L_{PP}	m	142.00	3.048
L_{WL}	m	142.18	3.052
B_{WL}	m	19.10	0.410
T_m	m	6.16	0.136
∇	m^3	8472	0.084
Δ	Ton	8684	0.086
C_B	-	0.506	0.506
A_{WP}	m^2		0.979
m	kg		82.55
x_G	m		-0.0157
y_G	m		0.0000
I_z	kg·m^2		49.99

Table 1 Full and model scale particulars.

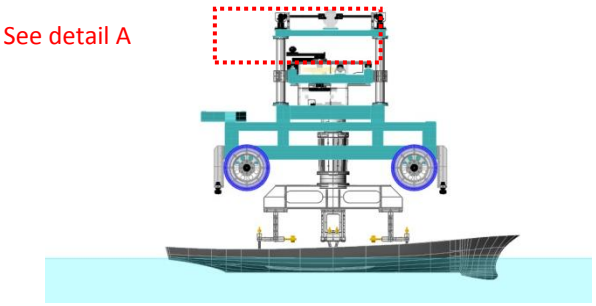

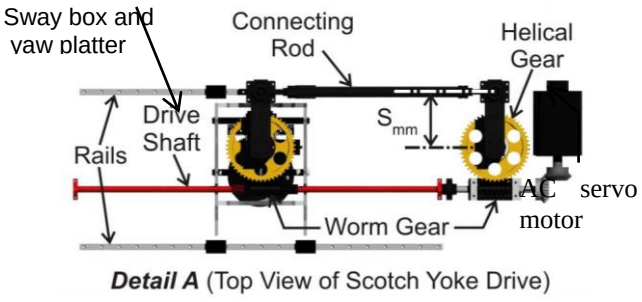

Figure 2 Side view of the PMM carriage and model ship mount (top), and close up of the scotch yoke drive (bottom).

The model is ballasted with respect to port and starboard draft markers, and then connected to a mount with three ball-bearing type contacts which allows the model to move freely in pitch and heave, but constrains roll motion (See Figure 2). The mount is suspended from the load cell which is fixed at the PMM carriage. The mass and yaw moment of inertia of the mount are measured to correct their effects on the measured forces and moment at the date reductions phase of the test.

Fr [-]	U_C [m/s]	β [deg.]	v' † [-]
0.280	1.531	-10	-0.174

† $v' = \frac{v}{U_C}$

Table 2 Test conditions for static drift test.

Fr [-]	U_C [m/s]	β_{corr}* [deg]	N [rpm]	S_{mm} [m]	v'_{max}† [-]	$\dot{v}'_{max}$‡ [-]
0.280	1.531	10	8.0210	0.1584	0.174	0.291

*$\beta_{corr} = \frac{v_{max}}{U}$, †$v'_{max} = \frac{v_{max}}{U}$, ‡$\dot{v}'_{max} = \frac{\dot{v}_{max} L_{PP}}{U}$

Table 3 Test conditions for pure sway test.

Fr [-]	U_C [m/s]	N [rpm]	S_{mm} [m]	ψ_0 [deg.]	r'_{max}† [--]	$\dot{r}'_{max}$‡ [--]
0.280	1.531	8.0210	0.1636	10.2	0.30	0.50

†$r'_{max} = \frac{r_{max} L_{PP}}{U}$, ‡$\dot{r}'_{max} = \frac{\dot{r}_{max} L_{PP}^2}{U^2}$

Table 4 Test conditions for pure yaw test.

Fr [-]	U_C [m/s]	β [deg]	N [rpm]	S_{mm} [m]	ψ_0 [deg]	r'_{max} [--]	$\dot{r}'_{max}$ [--]
0.280	1.531	10	8.0210	0.1636	10.2	0.30	0.50

Table 5 Test conditions for yaw and drift test.

Static drift test is conducted at the drift angle β = -10°; pure sway test at the corresponding drift angle β_{corr} = 10°; pure yaw test at r'_{max} = 0.3; and yaw and drift test at the same yaw rate of the pure yaw test with a drift angle β = 10°. The details of each test condition are presented in Tables 2 – 5. Test conditions in the present procedure are a part of the full test matrix in Yoon et al. (2007).

2. Data Acquisition and Reduction

The present interest is in data acquisition of carriage speed U_C, ship model motions (y, ψ), and forces and moments (F_x, F_y, M_z) for static and dynamic PMM tests. All variables are acquired as time histories through each carriage run. Static test variables (F_x, F_y, M_z) are time-averaged whereas dynamic test variables (y, ψ, F_x, F_y, M_z) are treated with harmonic analysis in the data reduction phases of the study. The measurement details for U_C are presented in Longo and Stern, (2005).

If it is assumed that the vessel moves in the horizontal plane only (surge, sway, and yaw), the motion equations are reduced to the following equations:

$$\begin{aligned} -F_x + X &= m(\dot{u} - vr - x_G r^2 - y_G \dot{r}) \\ -F_y + Y &= m(\dot{v} + ur - y_G r^2 + x_G \dot{r}) \\ -M_z + N &= I_z \dot{r} + m\big(x_G(\dot{v} + ur) - y_G(\dot{u} - rv)\big) \end{aligned} \quad (1)$$

where, X, Y, N are the hydrodynamic forces and moment, m is the mass of the model ship, I_z is the yaw moment of inertia of the model ship, x_G is the longitudinal distance from midship to model ship centre of gravity (COG), y_G is the transverse distance from centerplane to model ship COG, u, v, r are surge, sway, yaw velocities, respectively, $\dot{u}$, $\dot{v}$, $\dot{r}$ are surge, sway, yaw accelerations, respectively. In general y_G=0 for conventional marine vessels, but it is assumed to be non-zero for the purpose of uncertainty assessment. Equations (1) can be made non-dimensional using water density ρ, advance speed $U = \sqrt{u^2 + v^2}$, mean draft T_m, and ship model length L_{PP}. The non-dimensional variables are denoted with a prime symbol and represent the data reduction equations (DRE's) for the measurements herein.

$$X' = \frac{F_x + m(\dot{u} - vr - x_G r^2 - y_G \dot{r})}{1/2 \rho U^2 T_m L_{PP}} \quad (2)$$

$$Y' = \frac{F_y + m(\dot{v} + ur - y_G r^2 + x_G \dot{r})}{1/2 \rho U^2 T_m L_{PP}} \quad (3)$$

$$N' = \frac{M_z + I_z\dot{r} + m\left(x_G(\dot{v}+ur) - y_G(\dot{u}-rv)\right)}{1/2\rho U^2 T_m L_{PP}^2} \quad (4)$$

Although equations (2-4) are technically applicable DRE's for all tests herein, they can be simplified considerably by dropping the inertia terms for the case of the static drift tests which is done below in equations (5-7).

$$X' = \frac{F_x}{1/2\rho U_C^2 T_m L_{PP}} \quad (5)$$

$$Y' = \frac{F_y}{1/2\rho U_C^2 T_m L_{PP}} \quad (6)$$

$$N' = \frac{M_z}{1/2\rho U_C^2 T_m L_{PP}^2} \quad (7)$$

For static tests, average values of surge and sway forces and yaw moment are computed from the time histories. For the dynamic tests, first the inertia forces and moment of the model ship and the mount are subtracted from the measured forces and moment, respectively. Then, the resultant time histories of the forces and yaw moment are reconstructed with a 6th-order Fourier Series equation using the input PMM frequency as the prime frequency of the FS. Uncertainties related to the averaging and FS reconstruction processes are not considered in the present procedure. The choice for a 6th order Fourier series is a choice, made in this example, and may lead to a sensitivity of the derivatives related to small changes in the forces. In a fully worked out uncertainty analysis , the sensitivity to the choice of the order of the Fourier series can be taken into account.

3. Measurement Systems and Procedures

Three forces and three moments are measured with an Izumi six-component strain-gage type load cell, six Izumi amplifiers, 16-channel AD converter and PC. Maximum force and moment ranges are 500 N for F_x, F_y, F_z and 50 N-m, 50 N-m, 200 N-m for M_x, M_y, M_z, respectively.

Ship model motions are measured using a Krypton Electronic Engineering Rodym DMM motion tracker. The Rodym DMM is a camera-based measurement system that triangulates the position of a target in 3D space for contactless measurement and evaluation of 6DOF motions. The hardware consists of a camera module comprising three fixed CCD cameras, target with 1-256 light-emitting diodes (LED's), camera control unit, hand-held probe with six LED's, and PC. Krypton software is used for system calibration, and data acquisition and reduction.

Carriage speed is measured with an IIHR-designed and built speed circuit. The operating principle is integer pulse counting at a wheel-mounted encoder. The hardware consists of an 8000-count optical encoder, carriage wheel, sprocket pair and chain, analog-digital (AD) converter, and PC. Linear resolution of the encoder, sprocket pair and chain, and wheel assembly is 0.15 mm/pulse. The speed circuit is periodically bench-calibrated to determine and adjust the frequency input/voltage output transfer function.

A four-wheel carriage supports the main PMM mechanical system which is towed behind the IIHR drive carriage. The mechanical system is a scotch-yoke type which converts rotational motion of an 11 kW AC servo motor to linear sway motion of a sway box and angular yaw motion of a yaw platter beneath the sway box (See Figure 2). The scotch yoke is driven through a control rack, PC, and software up to 0.25 Hz with maximum sway and yaw amplitudes of ±500 mm and ±30°, respectively. A strongback (1.5 m) is attached to the yaw platter, which is pre-settable at a drift angle between ±30° for

static drift or combined yaw and drift tests. Factory calibrated linear and rotational potentiometers are installed on the carriage to monitor and report the sway and yaw position of the sway box and yaw platter, respectively.

For static drift tests, the ship motion is defined by the towing speed U_C and the specified drift angle β relative to the towing direction. For dynamic tests, the ship motion is imposed to control velocities (surge u, sway v, yaw r), and accelerations (surge $\dot{u}$, sway $\dot{v}$, yaw $\dot{r}$) in the local ship coordinate system at any given instant (See figure 3).

Dynamic test ship motions are composed of:

1) carriage speed, U_C;
2) PMM-generated transverse oscillation of the model from side to side (perpendicular to the towing direction) defined by the velocity v_{PMM} and the acceleration $\dot{v}_{PMM}$;
3) PMM-generated horizontal rotation from side to side of the model around a vertical axis through the mid ship, defined by the angular velocity r_{PMM} and the angular acceleration $\dot{r}_{PMM}$ and
4) a drift angle β if the yaw and drift condition is considered (Fig. 2). The time-dependent PMM motion parameters can differ from facility to facility, but those for the current example are described basically by three quantities. These include the sway crank amplitude S_{mm}, yaw motion amplitude ψ_0, and PMM frequency $\omega = 2\pi N/60$, where N is the number of PMM rotations per minute. The following relations are used to setup static and dynamic tests according to the test conditions in Tables 2-5:

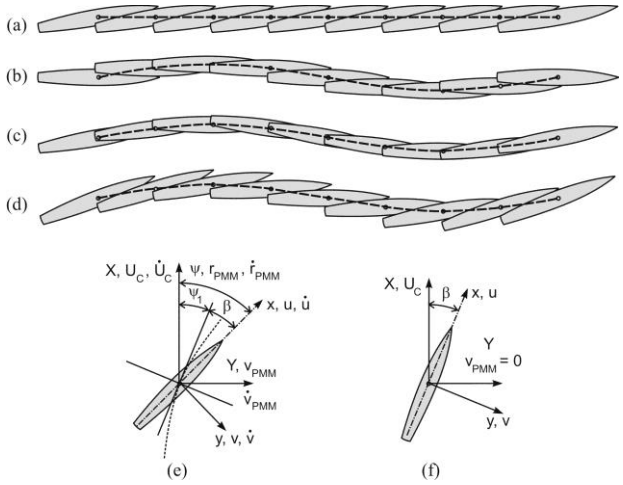

Figure 3 Definitions of PMM tests and motion parameters: (a) static drift; (b) pure sway; (c) pure yaw; (d) yaw and drift; (e) dynamic test motion parameters; (f) static test motion parameters.

Heading:

$$\psi = \psi_0 \cos \omega t + \beta \tag{8}$$

Yaw rate:

$$r_{PMM} = -\psi_0 \omega \sin \omega t \tag{9}$$

Yaw acceleration:

$$\dot{r}_{PMM} = -\psi_0 \omega^2 \cos \omega t \tag{10}$$

Transverse translation:

$$\eta_{PMM} = -2S_{mm} \sin \omega t \tag{11}$$

Transverse velocity:

$$v_{PMM} = -2\omega S_{mm} \cos \omega t \tag{12}$$

Transverse acceleration:

$$v_{PMM} = 2\omega^2 S_{mm} \sin \omega t \tag{13}$$

where, η_{PMM} in (11) is the transverse position of the model ship in towing tank coordinates. If a different PMM motion generation mechanism is used, equations (8) to (13) should be replaced with the appropriate PMM motion equations.

The motion parameters of the model ship moving in a ship-fixed moving frame of refer-

ence can be expressed with the above PMM motion parameters. The carriage acceleration is assumed to be zero, i.e. $\dot{U}_C = 0$ in the following equations.

Sway velocity:
$$v = v_{\mathrm{PMM}} \cos\psi - U_{\mathrm{C}} \sin\psi \quad (14)$$

Sway acceleration:
$$\dot{v} = \dot{v}_{\mathrm{PMM}} \cos\psi - r(U_{\mathrm{C}} \cos\psi + v_{\mathrm{PMM}} \sin\psi) \quad (15)$$

Yaw rate:
$$r = r_{\mathrm{PMM}} \quad (16)$$

Yaw acceleration:
$$\dot{r} = \dot{r}_{PMM} \quad (17)$$

Surge velocity:
$$u = U_C \cos\psi + v_{PMM} \sin\psi \quad (18)$$

Surge acceleration:
$$\dot{u} = \dot{v}_{PMM} \sin\psi + r(v_{PMM} \cos\psi - U_C \sin\psi) \quad (19)$$

4. Uncertainty Analysis

The uncertainty analysis procedures are based on estimates of type A and type B, and their root-sum-square (RSS) combination to ascertain expanded uncertainty (U). UA is applied to data reduction equations (2) – (4) for dynamic tests and (5) – (7) for static tests, respectively, which are written in functional forms below (20) – (22) for dynamic tests and (23) – (25) for static tests, respectively.

$$X' = X'\left(\begin{matrix}L_{\mathrm{PP}}, T_{\mathrm{m}}, x_{\mathrm{G}}, y_{\mathrm{G}}, m, \rho, \\ u, v, r, \dot{u}, \dot{r}, F_x\end{matrix}\right) \quad (20)$$

$$Y' = Y'\left(\begin{matrix}L_{\mathrm{PP}}, T_{\mathrm{m}}, x_{\mathrm{G}}, y_{\mathrm{G}}, m, \rho, \\ u, v, r, \dot{v}, \dot{r}, F_y\end{matrix}\right) \quad (21)$$

$$N' = N'\left(\begin{matrix}L_{\mathrm{PP}}, T_{\mathrm{m}}, x_{\mathrm{G}}, y_{\mathrm{G}}, m, I_Z, \rho, \\ u, v, r, \dot{u}, \dot{v}, \dot{r}, M_z\end{matrix}\right) \quad (22)$$

$$X' = X'(L_{\mathrm{PP}}, T_{\mathrm{m}}, \rho, U_{\mathrm{C}}, F_x) \quad (23)$$

$$Y' = Y'(L_{\mathrm{PP}}, T_{\mathrm{m}}, \rho, U_{\mathrm{C}}, F_y) \quad (24)$$

$$N' = N'(L_{\mathrm{PP}}, T_{\mathrm{m}}, \rho, U_{\mathrm{C}}, M_z) \quad (25)$$

Type B uncertainty is estimated with consideration of elemental uncertainty sources for individual variables, whereas type A uncertainty is estimated end to end. The expanded uncertainty is achieved through careful estimation of type B uncertainties and usage of a large sample, multiple test approach for type A uncertainties. The sources of uncertainty for PMM tests are shown in Figure 4.

4.1 Standard uncertainties (u)

Fourteen standard uncertainties U_x, where x = L_{PP}, T_{m}, x_{G}, y_{G}, m, I_Z, ρ, u, v, r, $\dot{u}$, $\dot{v}$, $\dot{r}$, F (hereafter F is either F_x, F_y, or M_z) are identified from the uncertainty propagation equations of the DRE's (20) – (22) for dynamic tests, and five standard uncertainties U_x, where x = L_{PP}, T_{m}, ρ, U_{C}, F from (23) – (25) for static tests.

$$U_R^2 = \sum_x \theta_x^2 U_x^2 \quad (26)$$

Sensitivity coefficients $\theta_x = \partial R/\partial x$ (hereafter R is either X', Y', or N') of individual variable results are evaluated analytically, and their definitions are summarized in Tables 12, 13, and 14 for $U_{X'}$, $U_{Y'}$, and $U_{N'}$, respectively. The individual uncertainties U_x are defined and estimated as below. Additional or details of estimation procedures for some variables are presented in Appendices B, C, D, and E.

The model length uncertainty is estimated as $U_{L_{\mathrm{PP}}}$= 0.002m, which corresponds to 0.07% of L_{PP}, by assuming the model ship fabrication uncertainty to be ±1 mm in all coordinates according to ITTC Procedure 7.5-01-01-01 Rev 01, 'Ship Models'.

U_{T_m} is composed of two uncorrelated uncertainties ($U_{T_\mathrm{m},1}$, $U_{T_\mathrm{m},2}$). $U_{T_\mathrm{m},1}$ is the marking accuracy of draft markers on the model ship surface, and assumed to be 0.1 mm. $U_{T_m,2}$ is from the model ship ballasting uncertainty with respect to the draft markers, which is estimated as 1 mm based on visual inspection. From the RSS of $U_{T_\mathrm{m},1}$ and $U_{T_\mathrm{m},2}$, U_{T_m} is estimated as 1 mm, which corresponds to 0.7% of T_m. The estimation procedure for the case of model ballasting based on displacement is given in Appendix B.

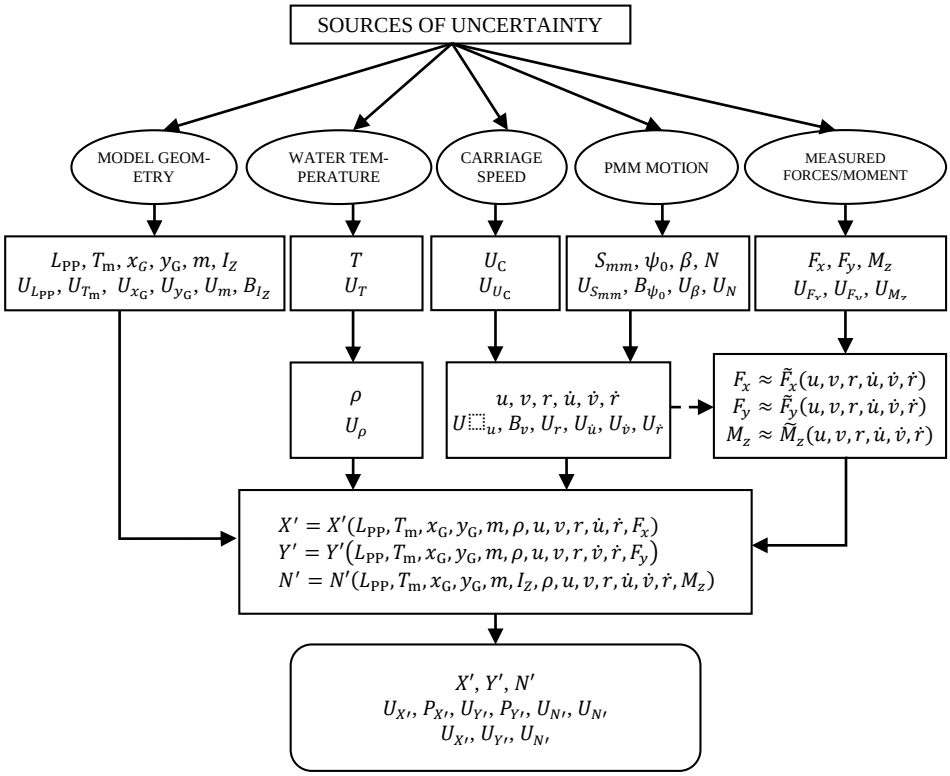

Figure 4 Sources of uncertainties in a PMM test.

The uncertainties of *COG* (U_{x_G}, U_{y_G}) consist of two uncorrelated uncertainties; $U_{G,1}$and $U_{G,2}$, where the subscript G represents either x_G or y_G. $U_{G,1}$ is the model installation uncertainty and $U_{\mathrm{G},2}$ is the deviation of actual model COG from the designed position. Estimated U_{x_G} and U_{y_G} are summarized as following:

Term (G)	$U_{G,1}$ [m]	$U_{G,2}$ [m]	U_G [m]
x_G	0.002	0.005	0.0054
y_G	0.001	0.002	0.0022

Total mass m of the model is calculated by summing individually measured element masses which are the bare model ship, ballast weights, and parts for model installation. Accordingly, U_m is the RSS of $U_{m,i}$'s which are the individual mass measurement uncertainties. U_m is estimated as 0.11 kg (0.1% of m=82.55 kg). Measured masses of all elements together with their uncertainties are summarized in Table 6.

From separate measurements of model ship yaw moment of inertia, U_{I_z} is estimated as 1.84 kg·m^2, which corresponds to 3.7 % of the measured model yaw moment of inertia I_z = 49.79 kg·m^2. Details of I_z measurement and U_{I_z} estimation procedures are given in Appendix C.

Water density is calculated according to the ITTC procedure 7.5-02-01-03, which indicates that the water density is a function of the temperature.

Water temperature T is measured at the model mid draft with a resistive-type probe and signal conditioner. The temperature-probe accuracy is rated at U_T = ±0.2°C and $U_\rho = \sqrt{(\partial\rho/\partial T)^2 U_T^2}$ is estimated as 0.041 kg/m^3 which is 0.004% of the measured water density ρ = 998.1 kg/m^3 at 20°C.

No. (i)	Item	m_i [kg]	$u(m_i)$ [kg]
1	Bare model ship	55.99	0.045
2	Ballast weight 1	2.27	0.023
3	Ballast weight 6	2.27	0.023
4	Ballast weight 11	2.27	0.023
5	Ballast weight 12	2.27	0.023
6	Ballast weight 13	2.27	0.023
7	Ballast weight 15	1.70	0.023
8	Ballast weight 16	1.70	0.023
9	Ballast weight 18	1.13	0.023
10	Ballast weight 19	1.09	0.023
11	Ballast weight 23	1.13	0.023
12	Ballast weight 24	0.88	0.023
13	Ballast weight A	0.20	0.023
14	Ballast weight B	0.20	0.023
15	Ballast weight C	1.36	0.023
16	Krypton target	2.47	0.023
17	Part 1	1.11	0.023
18	Part 2	1.11	0.023
19	Part 3	1.11	0.023
$m = \sum_i m_i$ = 82.55Kg			
$U_m = \sqrt{\sum_i U_{m_i}^2}$ = 0.11Kg			

Table 6 Model mass uncertainties estimation.

Carriage speed uncertainty is estimated end-to-end by calibrating the carriage speed with respect to reference speeds. Reference speeds are obtained by measuring travel time Δt for a known distance ΔL. From the calibration U_{U_C} is estimated as 0.010m/s, which corresponds to 0.7% of carriage speed 1.531m/s (Fr = 0.280). Details of U_C calibration and U_{U_C} estimation procedures are summarized in Appendix D.

Uncertainties of motion parameters U_v, $U_{\dot{v}}$, U_r, $U_{\dot{r}}$, U_u, $U_{\dot{u}}$ are estimated from combined uncertainty, using equations (28) – (33) through their own DRE's (14) – (19), respectively.

$$U_v^2 = \theta_{U_C}^2 U_{U_C}^2 + \theta_\psi^2 U_\psi^2 + \theta_{v_{\mathrm{PMM}}}^2 U_{v_{\mathrm{PMM}}}^2 \quad (27)$$

$$U_{\dot{v}}^2 = \theta_{U_C}^2 U_{U_C}^2 + \theta_\psi^2 U_\psi^2 + \theta_r^2 U_r^2 + \theta_{v_{\mathrm{PMM}}}^2 U_{v_{\mathrm{PMM}}}^2 + \theta_{\dot{v}_{\mathrm{PMM}}}^2 U_{\dot{v}_{\mathrm{PMM}}}^2 \quad (28)$$

$$U_r^2 = \theta_{\psi_0}^2 U_{\psi_0}^2 + \theta_N^2 U_N^2 + \theta_t^2 U_t^2 \quad (29)$$

$$U_{\dot{r}}^2 = \theta_{\psi_0}^2 U_{\psi_0}^2 + \theta_N^2 U_N^2 + \theta_t^2 U_t^2 \quad (30)$$

$$U_u^2 = \theta_{U_C}^2 U_{U_C}^2 + \theta_\psi^2 U_\psi^2 + \theta_{v_{\mathrm{PMM}}}^2 U_{v_{\mathrm{PMM}}}^2 \quad (31)$$

$$U_{\dot{u}}^2 = \theta_{U_C}^2 U_{U_C}^2 + \theta_\psi^2 U_\psi^2 + \theta_r^2 U_r^2 + \theta_{v_{\mathrm{PMM}}}^2 U_{v_{\mathrm{PMM}}}^2 + \theta_{\dot{v}_{\mathrm{PMM}}}^2 U_{\dot{v}_{\mathrm{PMM}}}^2 \quad (32)$$

where the uncertainties, U_ψ, $U_{v_{\mathrm{PMM}}}$, $U_{\dot{v}_{\mathrm{PMM}}}$ are estimated from their data reduction equations (19), (23), (24), respectively.

$$U_\psi^2 = \theta_{\psi_0}^2 U_{\psi_0}^2 + \theta_N^2 U_N^2 + \theta_t^2 U_t^2 + \theta_\beta^2 U_\beta^2 \quad (33)$$

$$U_{v_{\mathrm{PMM}}}^2 = \theta_N^2 U_N^2 + \theta_{S_{\mathrm{mm}}}^2 U_{S_{\mathrm{mm}}}^2 + \theta_t^2 U_t^2 \quad (34)$$

$$U_{\dot{v}_{\mathrm{PMM}}}^2 = \theta_N^2 U_N^2 + \theta_{S_{\mathrm{mm}}}^2 U_{S_{\mathrm{mm}}}^2 + \theta_t^2 U_t^2 \quad (35)$$

The sensitivity coefficients in (28) – (36) are evaluated analytically. Of the five elemental uncertainties associated with motion parameters U_x, where x= S_{mm}, N, t, β, ψ_0, $U_{S_{\mathrm{mm}}}$ is from the test setup and U_N, U_t are from empirical estimation, which are presented in Table 7. Drift angle uncertainty U_β is assumed to be composed

of two uncorrelated elemental uncertainties $U_{\beta,\text{align}}$ and $U_{\beta,\text{drift}}$. $U_{\beta,\text{align}}$ is the model ship installation uncertainty with respect to straight towing direction and assumed to be 0.03°. $U_{\beta,\text{drift}}$ is the deviation from designated drift angle setting and estimated end-to-end by calibrating the drift angle with respect to reference angles, and estimated as 0.22°. Details of drift angle calibration and U_β estimation procedures are presented in the Appendix E. The uncertainty of the maximum heading angle of yaw motion U_{ψ_0} is assumed to be same as U_β.

Uncertainty	Magnitude
$U_{S_{\text{mm}}}$	0.0005 m
$U_\beta = U_{\psi_0}$	0.22 deg
U_{N}	0.0006 rpm
U_t	0.001 sec

Table 7 Elemental uncertainties related to the PMM motion generation.

Uncertainties of measured forces/moment U_F, where F is either F_x, F_y, or M_z, is composed of 9 uncorrelated elemental uncertainties for dynamic tests

$$U_F^2 = U_{F,\text{calib}}^2 + U_{F,\text{acquis}}^2 + U_{F,u}^2 + U_{F,\dot{u}}^2 + U_{F,v}^2 + U_{F,\dot{v}}^2 + U_{F,r}^2 + U_{F,\dot{r}}^2 + U_{F,t}^2 \quad (36)$$

and 4 uncorrelated elemental uncertainties for static tests.

$$U_F^2 = U_{F,\beta}^2 + U_{F,\text{align}}^2 + U_{F,\text{calib}}^2 + U_{F,\text{acquis}}^2 \quad (37)$$

$U_{F,\beta}$ and $U_{F,\text{align}}$ are from drift angle setting uncertainty and uncertainty of alignment of ship model with respect to straight towing direction, respectively. Estimation procedures and results of $U_{F,\beta}$ and $U_{F,\text{align}}$ are summarized in Table 8. Sensitivity coefficients $\partial F/\partial\beta$'s are obtained from static drift test results. $U_{F,\text{calib}}$ is the RSS of the uncertainties of individual weights used for forces/moment gauge calibration.

ε_β [rad]	$\varepsilon_{\text{align}}$ [rad]	β = -10°		
3.84× 10^{-3}	5.24× 10^{-4}	$\frac{dF_x}{d\beta}$	$U_{F_x,\beta}$	$U_{F_x,\text{align}}$
		[N/rad]	[N]	[N]
		30.2	0.1161	0.0158
		$\frac{dF_y}{d\beta}$	$U_{F_y,\beta}$	$U_{F_y,\text{align}}$
		[N/rad]	[N]	[N]
		209.9	0.8061	0.1100
		$\frac{dM_z}{d\beta}$	$U_{M_z,\beta}$	$U_{M_z,\text{align}}$
		[Nm/rad]	[Nm]	[Nm]
		283.9	1.0903	0.1488
$U_{F,\beta}^2 = \left(\frac{dF}{d\beta}\right)^2 \varepsilon_\beta^2$, $U_{F,\text{align}}^2 = \left(\frac{dF}{d\beta}\right)^2 \varepsilon_{F,\text{align}}^2$; $F = F_x$, F_{yY}, or M_z				

Table 8 $U_{F,\beta}$ and $U_{F,\text{align}}$ estimations.

Estimation procedures and measurement results of $U_{F,\text{calib}}$ are summarized in Table 9.

F_x weight, w_i [N]	$\varepsilon_{w,i}$ [N]	F_y weight, w_i [N]	$\varepsilon_{w,i}$ [N]
9.81	0.00020	4.90	0.00010
14.71	0.00029	9.81	0.00020
19.61	0.00039	14.71	0.00029
49.03	0.00098	19.61	0.00039
-	-	49.03	0.00098
$U_{F,\text{calib}} = \sqrt{\sum_i \varepsilon_{w,i}^2}$ $U_{F_x,\text{calib}} = U_{F_y,\text{calib}} = 0.001\text{N}$			

Table 9a $U_{F_X,\text{calib}}$ and $U_{F_Y,\text{calib}}$ estimation.

weight, w_i [N]	$M_{z,\text{calib},i}$ [Nm]	ε_{w_i} [N]	$U_{M_z,\text{calib},i}$ [Nm]
4.90	2.24	0.00010	0.00245
9.81	4.48	0.00020	0.00490
14.71	6.73	0.00029	0.00736
19.61	8.97	0.00039	0.00981
49.03	22.42	0.00098	0.02452

L_{calib} = 0.4572m, $\varepsilon_{L_{\text{calib}}}$ = 0.0005m

$$M_{z,\text{calib},i} = w_i \times L_{\text{calib}}$$

$$U^2_{M_z,\text{calib},i} = \left(\frac{\partial M_{z,\text{calib},i}}{\partial w_i}\right)^2 \varepsilon^2_{w_i} + \left(\frac{\partial M_{z,\text{calib},i}}{\partial L_{\text{calib}}}\right)^2 \varepsilon^2_{L_{\text{calib}}} = L^2_{\text{calib}}\varepsilon^2_{w_i} + \varepsilon^2_{w_i}\varepsilon^2_{L_{\text{calib}}}$$

$$U_{M_z,\text{calib}} = \sqrt{\sum_i U^2_{M_z,\text{calib},i}} = 0.028\text{Nm}$$

Table 9b $U_{M_z,\text{calib}}$ estimation.

F_x		F_y		M_z	
$\lvert F_x\rvert$ [N]	$\lvert\overline{\Delta F_x}\rvert_{\max}$ [N]	$\lvert F_y\rvert$ [N]	$\lvert\overline{\Delta F_y}\rvert_{\max}$ [N]	$\lvert M_z\rvert$ [Nm]	$\lvert\overline{\Delta M_z}\rvert_{\max}$ [Nm]
9.81	0.0282	9.81	0.0262	8.97	0.0352
14.71	0.0407	19.61	0.0558	14.93	0.0494
19.61	0.0571	39.23	0.1334	26.90	0.0782
29.42	0.0769	58.84	0.2009	35.87	0.1045
49.03	0.1326	78.45	0.2767	44.84	0.1389

$$\lvert\overline{\Delta F}\rvert_{\max} = \lvert\overline{\Delta F}\rvert + U_{\lvert\overline{\Delta F}\rvert}$$

$$U_{\lvert\overline{\Delta F}\rvert} = \frac{2S_{\lvert\overline{\Delta F}\rvert}}{\sqrt{M}},\ S_{\lvert\overline{\Delta F}\rvert} = \left[\sum_{i=1}^{M} \frac{(\lvert\Delta F_i\rvert - \lvert\overline{\Delta F}\rvert)^2}{M-1}\right]^{\frac{1}{2}}$$

$$\overline{\Delta F} = \frac{1}{M}\sum_{i=1}^{M}\lvert\Delta F_i\rvert,\ \Delta F_i = F_{\text{measured},i} - F_{\text{applied},i}$$

M : number of repeats = 12

$U_{F_x,\text{acquis}}$ = 0.002634$\lvert F_x\rvert$ + 0.002534

$U_{F_y,\text{acquis}}$ = 0.003668$\lvert F_y\rvert$ + 0.001245

$U_{M_z,\text{acquis}}$ = 0.002927$\lvert M_z\rvert$ + 0.002505

Table 10 $U_{\text{F,acquis}}$ estimation.

$U_{F,\text{acquis}}$ is from the volt-to-force conversion uncertainty of the forces/moment measurement gauges. Estimation procedures and measurement results of $U_{F,acquis}$ are summarized in Table 10. These are based on repeat tests.

Other standard uncertainties $U_{F,u}$, $U_{F,\dot{u}}$, $U_{F,v}$, $U_{F,\dot{v}}$, $U_{F,r}$, $U_{F,\dot{r}}$, $U_{F,t}$ are calculated by applying the uncertainty propagation equation to measured forces and moment F by assuming F is a function of motion parameters $(u, v, r, \dot{u}, \dot{v}, \dot{r})$ and time (t),

$$U_{F,x} = \frac{\partial F}{\partial x} U_x \tag{38}$$

where $x = u, v, r, \dot{u}, \dot{v}, \dot{r}, t$.

Pure yaw	$\tilde{F}_x = X_0 + X_u u + X_r r + X_{rr} r^2 + X_{\dot{u}}\dot{u} + X_{\dot{r}}\dot{r} + X_v v + X_{\dot{v}}\dot{v}$ $\tilde{F}_y = Y_0 + Y_u u + Y_r r + Y_{rrr} r^3 + Y_{\dot{u}}\dot{u} + Y_{\dot{r}}\dot{r} + Y_v v + Y_{\dot{v}}\dot{v}$ $\tilde{M}_z = M_0 + M_u u + M_r r + M_{rrr} r^3 + M_{\dot{u}}\dot{u} + M_{\dot{r}}\dot{r} + M_v v + M_{\dot{v}}\dot{v}$
Pure sway	$\tilde{F}_x = X_0 + X_u u + X_r r + X_{\dot{u}}\dot{u} + X_{\dot{r}}\dot{r} + X_v v + X_{\dot{v}}\dot{v} + X_{vv} v^2$ $\tilde{F}_y = Y_0 + Y_u u + Y_r r + Y_{\dot{u}}\dot{u} + Y_{\dot{r}}\dot{r} + Y_v v + Y_{\dot{v}}\dot{v} + Y_{v\lvert v\rvert} v\lvert v\rvert$ $\tilde{M}_z = M_0 + M_u u + M_r r + M_{\dot{u}}\dot{u} + M_{\dot{r}}\dot{r} + M_v v + M_{\dot{v}}\dot{v} + M_{v\lvert v\rvert} v\lvert v\rvert$
Yaw and drift	$\tilde{F}_x = X_0 + X_u u + X_r r + X_{rr} r^2 + X_{\dot{u}}\dot{u} + X_{\dot{r}} r + \dot{X}_{\dot{v}}\dot{v} + X_v v + X_{vr} vr + X_{uu} u^2 + X_{vv} v^2 + X_{uv} uv$ $\tilde{F}_y = Y_0 + Y_u u + Y_r r + Y_{rrr} r^3 + Y_{\dot{u}}\dot{u} + Y_v v + Y_{vu} vu + Y_{v\lvert v\rvert} v\lvert v\rvert + Y_{v\lvert r\rvert} v\lvert r\rvert + Y_{r\lvert v\rvert} r\lvert v\rvert + Y_{rvv} rv^2 + Y_{vrr} vr^2$ $\tilde{M}_z = M_0 + M_u u + M_r r + M_{rrr} r^3 + M_{\dot{u}}\dot{u} + M_v v + M_{vu} vu + M_{rvv} rv^2 + M_{vrr} vr^2 + M_{v\lvert v\rvert} v\lvert v\rvert + M_{v\lvert r\rvert} v\lvert r\rvert + M_{r\lvert v\rvert} r\lvert v\rvert$

Table 11 Definitions of polynomial models.

Due to the absence of data reduction equations for those variables, measured forces/moment F are approximated as a polynomial expansion model $\tilde{F}$ of the variables.

$$F \approx \tilde{F} = \sum_k \sum_{n=1}^{J} A_{k,n}(x_k)^n \tag{39}$$

where, n=0, 1, …, J; x_k= u, v, r, $\dot{u}$, $\dot{v}$, $\dot{r}$; $A_{k,n}$ is the constant coefficient of n^{th} order x_k variable which is a function of time t. The number of variables k employed and/or the highest order J of each variable varies with each force component and type of test. The polynomial model definition for all forces/moment components for all test types of the UA test cases are summarized in Table 11.

With the polynomial modelling of the measured forces or moment the uncertainties in the equation (39) are evaluated

$$U_{F,x} = \frac{\partial F}{\partial x} U_x \approx \frac{\partial \tilde{F}}{\partial x} U_x \tag{40}$$

The coefficients of each polynomial model are calculated with the Least-Square fitting method. In equations (39) and (41) the standard uncertaintiesU_v, $U_{\dot{v}}$, U_r, $U_{\dot{r}}$, U_u, $U_{\dot{u}}$ are identical with the uncertainties defined in (28) to (33), respectively. With respect to $U_{F,t}$, the sensitivity coefficient $\partial F/\partial t$ is calculated numerically from the measured time histories of F.

4.2 Repeatability of measurement results

The uncertainties are determined from 12 repeat tests. The datasets are spaced in time at least 12 minutes between tests to minimize flow disturbances from previous runs, while spanning over a time period, usually one day, that is large relative to time scales of the factors that influence variability of the measurements. The same model ship, PMM motion generator, load cell, and motion tracker are used for the repeat tests due to limitations of time and experiment resources. The model is not dismounted and re-installed during the repeat tests. However, the PMM motion control parameters, such as drift angle, sway crank amplitude, or maximum heading angle settings are changed between tests. The uncertainties are computed with the standard multiple-test equation

$$U_{\bar{R}} = \frac{\mathrm{k} S_{\bar{R}}}{\sqrt{12}} \tag{41}$$

where R= X', Y', N' and the coverage factor k=2 to obtain the expanded uncertainty. $S_{\bar{R}}$ is the standard deviation defined as

$$S_{\bar{R}} = \left[\sum_{k=1}^{12} \frac{(R_k - \bar{R})}{11}\right]^{\frac{1}{2}} \tag{42}$$

and

$$\bar{R} = \frac{1}{12} \sum_{k=1}^{12} R_k \tag{43}$$

where, R_k is either X', Y', or N' of the k^{th} run, which are defined in (2) – (4) for dynamic tests and (5) – (7) for static tests, respectively.

4.3 Results

The uncertainty assessment results are presented in Table 15 for static drift tests and Tables 16 - 18 for dynamic tests. Each table consists of three parts;

- DRE variables and their uncertainty contributions to the expanded uncertainty of non-dimensional forces and moment U_R(top),
- uncertainties of measured forces and moments U_F including contributions from elemental uncertainties$U_{F,x}$ (middle), and
- total uncertainties their contributions to total expanded uncertainty U_{95R} (bottom).

The latter includes scaled total uncertainties in percentile of either variable magnitude or its dynamic range.

For dynamic tests the UA results only at their maximum motions are presented and compared in the tables.

Static tests From Table 15 (top) the largest bias is the carriage speed U_{U_C} and the second largest uncertainty is the measured force U_F for X', while U_F is the largest uncertainty and U_{U_C} is the second largest uncertainty for Y' and N'. The measured forces/moment bias U_F, a common large uncertainty for X', Y', N', is mainly from the uncertainty in drift angle $U_{F,\beta}$ as presented in Table 15 (middle). $U_{F,\beta}$ contributes over 90% to U_F for all cases. From Table 15 (bottom), the total uncertainty U_R contributes over 90%, and the precision limit P_R contributes less than 10% to U_R, indicating most DRE variable results are highly repeatable. Total uncertainties U_R's are reasonably small, 1.9%, 3.4%, and 2.8% of X', Y', and N', respectively. Although the static drift tests are similar with the resistance test, a steady straight towing test, additional uncertainties from the drift angle setting associated with static drift test might explain the higher uncertainty levels. Improvements of static drift test uncertainty can be achieved by improving the carriage speed control for X' and drift angle setting accuracy for Y' and N', which are the biggest uncertainty sources.

Dynamic tests For pure yaw tests (Table 16), the primary bias is surge velocity B_u and the secondary is measured forces/moment B_F for X', B_F is the primary bias and the yaw rate B_r is secondary bias for Y', and again B_F is the primary and B_u is the secondary biases for N', respectively. The measured forces/moment bias B_F is composed largely of surge velocity $B_{F,u}$ and acceleration $B_{F,\dot{u}}$ for F_x, and of the yaw rate $B_{F,r}$ for F_y and M_z, respectively. The type B uncertainty P_X, is dominant (75%) for X', but the type A uncertainty B_Y, and B_N, are dominant (> 90%) for Y' and N'. The total uncertainty U_X, is 8% of X', and U_Y, and U_N, are 5%, and 1.4% of the dynamic ranges of Y' and N', respectively.

For pure sway test (Table 17), the surge velocity B_u is the primary source of uncertainty and measured force B_F and mean draft B_{T_m} are secondary source of uncertainty for X', B_F is the primary source of uncertainty and B_u is the secondary source of uncertainty for Y' and N', respectively. $B_{L_{PP}}$, B_{x_G}, B_{y_G}, B_m, B_{I_z}, B_ρ, B_v, B_r, $B_{\dot{u}}$, $B_{\dot{v}}$, $B_{\dot{r}}$ all contribute small or negligibly for all cases. The measured forces/moment bias B_F is composed mainly of the sway velocity $B_{F,v}$ for all F, but also from $B_{F,\text{acquis}}$ and $B_{F,u}$ for B_{F_x}. U_X, is 5.8% of X', and U_Y, and U_N, are all 2.1% of the dynamic ranges of Y' and N', respectively.

For yaw and drift tests (Table 18), the surge velocity B_u is the primary source of uncertainty and the measured forces/moment B_F is the secondary source of uncertainty for X', B_F is the primary and the yaw rate B_r is the secondary source of uncertainty for Y', and B_F is primary and B_u is the secondary source of uncertainty for N', respectively. The total uncertainty U_X, is about 7% of X', U_Y, and U_N, are 3.6% and 1.5% of the dynamic ranges of Y' and N', respectively.

In conclusion for the dynamic tests, primary source of uncertainty vary according to type of the test while the measured forces/moment source of uncertainty B_F is the common largest source of uncertainty. Ship model geometry related source of uncertainty and water density source of uncertainty are contributing small or negligibly except for the mean draft bias B_{T_m} and the longitudinal COG bias B_{x_G}. However, the uncertainties from motion parameters and

measured forces/moment are dominant according to forces/moment component and test type. For the dynamic tests, the total uncertainties U_R's are varying 6% ~ 8% of X', 1% ~ 5% of Y' and N' according to test type, which are larger than those of the static drift test results. Of the four different types of dynamic PMM tests, the pure yaw test total uncertainty is relatively higher than other kinds of PMM tests. The uncertainty of the dynamic test results can be improved by improving carriage speed control and increasing the number of repeat to reduce the type B uncertainty for X', and by improving the PMM motion control to reduce type A uncertainty for Y' and N', respectively.

	Dynamic Tests	Static Tests
θ_{F_x}	$\frac{2}{\rho(u^2+v^2)T_{\mathrm{m}}L_{\mathrm{PP}}}$	$\frac{2}{\rho U_C^2 T_{\mathrm{m}} L_{\mathrm{PP}}}$
θ_{ρ}	$\frac{-2\left(F_x+m\left(\dot{u}-rv-x_{\mathrm{G}}r^2-y_{\mathrm{G}}\dot{r}\right)\right)}{\rho^2(u^2+v^2)T_{\mathrm{m}}L_{\mathrm{PP}}}$	$\frac{-2F_x}{\rho^2 U_C^2 T_{\mathrm{m}} L_{\mathrm{PP}}}$
$\theta_{T_{\mathrm{m}}}$	$\frac{-2\left(F_x+m\left(\dot{u}-rv-x_{\mathrm{G}}r^2-y_{\mathrm{G}}\dot{r}\right)\right)}{\rho(u^2+v^2)T_{\mathrm{m}}^2L_{\mathrm{PP}}}$	$\frac{-2F_x}{\rho U_C^2 T_{\mathrm{m}}^2 L_{\mathrm{PP}}}$
$\theta_{L_{\mathrm{PP}}}$	$\frac{-2\left(F_x+m\left(\dot{u}-rv-x_{\mathrm{G}}r^2-y_{\mathrm{G}}\dot{r}\right)\right)}{\rho(u^2+v^2)T_{\mathrm{m}}L_{\mathrm{PP}}^2}$	$\frac{-2F_x}{\rho U_C^2 T_{\mathrm{m}} L_{\mathrm{PP}}^2}$
$\theta_{U_{\mathrm{C}}}$	-	$\frac{-4F_x}{\rho U_C^3 T_{\mathrm{m}} L_{\mathrm{PP}}}$
θ_m	$\frac{2\left(\dot{u}-rv-x_{\mathrm{G}}r^2-y_{\mathrm{G}}\dot{r}\right)}{\rho(u^2+v^2)T_{\mathrm{m}}L_{\mathrm{PP}}}$	-
θ_{x_G}	$\frac{-2mr^2}{\rho(u^2+v^2)T_{\mathrm{m}}L_{\mathrm{PP}}}$	-
θ_{y_G}	$\frac{-2m\dot{r}}{\rho(u^2+v^2)T_{\mathrm{m}}L_{\mathrm{PP}}}$	-
θ_u	$\frac{-4u\left(F_x+m\left(\dot{u}-rv-x_{\mathrm{G}}r^2-y_{\mathrm{G}}\dot{r}\right)\right)}{\rho(u^2+v^2)^2T_{\mathrm{m}}L_{\mathrm{PP}}}$	-
$\theta_{\dot{u}}$	$\frac{-2m}{\rho(u^2+v^2)T_{\mathrm{m}}L_{\mathrm{PP}}}$	-
θ_v	$\frac{2}{\rho(u^2+v^2)T_{\mathrm{m}}L_{\mathrm{PP}}}\left[-mr-\frac{2v\left(F_x+m\left(\dot{u}-rv-x_{\mathrm{G}}r^2-y_{\mathrm{G}}\dot{r}\right)\right)}{(u^2+v^2)}\right]$	-
θ_r	$\frac{-2m(v+2x_{\mathrm{G}}r)}{\rho(u^2+v^2)T_{\mathrm{m}}L_{\mathrm{PP}}}$	-
$\theta_{\dot{r}}$	$\frac{-2my_{\mathrm{G}}}{\rho(u^2+v^2)T_{\mathrm{m}}L_{\mathrm{PP}}}$	-

Table 12 Definitions of sensitivity coefficients for $U_{X'}$.

	Dynamic Tests	Static Tests
θ_{F_y}	$\frac{2}{\rho(u^2+v^2)T_{\mathrm{m}}L_{\mathrm{PP}}}$	$\frac{2}{\rho U_C^2 T_{\mathrm{m}} L_{\mathrm{PP}}}$
θ_{ρ}	$\frac{-2\left(F_y+m\left(\dot{v}+ru-y_{\mathrm{G}}r^2+x_{\mathrm{G}}\dot{r}\right)\right)}{\rho^2(u^2+v^2)T_{\mathrm{m}}L_{\mathrm{PP}}}$	$\frac{-2F_y}{\rho^2 U_C^2 T_{\mathrm{m}} L_{\mathrm{PP}}}$
$\theta_{T_{\mathrm{m}}}$	$\frac{-2\left(F_y+m\left(\dot{v}+ru-y_{\mathrm{G}}r^2+x_{\mathrm{G}}\dot{r}\right)\right)}{\rho(u^2+v^2)T_{\mathrm{m}}^2L_{\mathrm{PP}}}$	$\frac{-2F_y}{\rho U_C^2 T_{\mathrm{m}}^2 L_{\mathrm{PP}}}$
$\theta_{L_{\mathrm{PP}}}$	$\frac{-2\left(F_y+m\left(\dot{v}+ru-y_{\mathrm{G}}r^2+x_{\mathrm{G}}\dot{r}\right)\right)}{\rho(u^2+v^2)T_{\mathrm{m}}L_{\mathrm{PP}}^2}$	$\frac{-2F_y}{\rho U_C^2 T_{\mathrm{m}} L_{\mathrm{PP}}^2}$
$\theta_{U_{\mathrm{C}}}$	-	$\frac{-4F_y}{\rho U_C^3 T_{\mathrm{m}} L_{\mathrm{PP}}}$
θ_m	$\frac{2\left(\dot{v}+ru-y_{\mathrm{G}}r^2+x_{\mathrm{G}}\dot{r}\right)}{\rho(u^2+v^2)T_{\mathrm{m}}L_{\mathrm{PP}}}$	-
$\theta_{x_{\mathrm{G}}}$	$\frac{2m\dot{r}}{\rho(u^2+v^2)T_{\mathrm{m}}L_{\mathrm{PP}}}$	-
$\theta_{y_{\mathrm{G}}}$	$\frac{-2mr^2}{\rho(u^2+v^2)T_{\mathrm{m}}L_{\mathrm{PP}}}$	-
θ_u	$\frac{2}{\rho(u^2+v^2)T_{\mathrm{m}}L_{\mathrm{PP}}}\left[mr-\frac{2u\left(F_y+m\left(\dot{v}+ru-y_{\mathrm{G}}r^2+x_{\mathrm{G}}\dot{r}\right)\right)}{(u^2+v^2)}\right]$	-
θ_v	$\frac{-4v\left(F_y+m\left(\dot{v}+ru-y_G r^2+x_G\dot{r}\right)\right)}{\rho(u^2+v^2)^2T_mL_{PP}}$	-
$\theta_{\dot{v}}$	$\frac{2m}{\rho(u^2+v^2)T_{\mathrm{m}}L_{\mathrm{PP}}}$	-
θ_r	$\frac{2m(u-2y_{\mathrm{G}}r)}{\rho(u^2+v^2)T_{\mathrm{m}}L_{\mathrm{PP}}}$	-
$\theta_{\dot{r}}$	$\frac{2mx_{\mathrm{G}}}{\rho(u^2+v^2)T_{\mathrm{m}}L_{\mathrm{PP}}}$	-

Table 13 Definitions of sensitivity coefficients for $\mathbf{U_{Y'}}$.

	Dynamic Tests	Static Tests
θ_{M_z}	$\frac{2}{\rho(u^2+v^2)T_{\mathrm{m}}L_{\mathrm{PP}}^2}$	$\frac{2}{\rho U_{\mathrm{C}}^2 T_{\mathrm{m}} L_{\mathrm{PP}}^2}$
θ_{ρ}	$\frac{-2\left(M_z+I_z\dot{r}+m\left(x_{\mathrm{G}}(\dot{v}+ru)-y_{\mathrm{G}}(\dot{u}-rv)\right)\right)}{\rho^2(u^2+v^2)T_{\mathrm{m}}L_{\mathrm{PP}}^2}$	$\frac{-2M_z}{\rho^2 U_{\mathrm{C}}^2 T_{\mathrm{m}} L_{\mathrm{PP}}^2}$
$\theta_{T_{\mathrm{m}}}$	$\frac{-2\left(M_z+I_z\dot{r}+m\left(x_{\mathrm{G}}(\dot{v}+ru)-y_{\mathrm{G}}(\dot{u}-rv)\right)\right)}{\rho(u^2+v^2)T_{\mathrm{m}}^2L_{\mathrm{PP}}^2}$	$\frac{-2M_z}{\rho U_{\mathrm{C}}^2 T_m^2 L_{PP}^2}$
$\theta_{L_{\mathrm{PP}}}$	$\frac{-4\left(M_z+I_z\dot{r}+m\left(x_{\mathrm{G}}(\dot{v}+ru)-y_{\mathrm{G}}(\dot{u}-rv)\right)\right)}{\rho(u^2+v^2)T_{\mathrm{m}}L_{\mathrm{PP}}^3}$	$\frac{-4M_z}{\rho U_{\mathrm{C}}^2 T_m L_{PP}^3}$
$\theta_{U_{\mathrm{C}}}$	-	$\frac{-4M_z}{\rho U_{\mathrm{C}}^3 T_m L_{PP}^2}$
θ_{I_z}	$\frac{2\dot{r}}{\rho(u^2+v^2)T_{\mathrm{m}}L_{\mathrm{PP}}^2}$	-
θ_m	$\frac{2\left(x_{\mathrm{G}}(\dot{v}+ru)-y_{\mathrm{G}}(\dot{u}-rv)\right)}{\rho(u^2+v^2)T_{\mathrm{m}}L_{\mathrm{PP}}^2}$	-
$\theta_{x_{\mathrm{G}}}$	$\frac{2m(\dot{v}+ru)}{\rho(u^2+v^2)T_{\mathrm{m}}L_{\mathrm{PP}}^2}$	-
$\theta_{y_{\mathrm{G}}}$	$\frac{-2m(\dot{u}-rv)}{\rho(u^2+v^2)T_{\mathrm{m}}L_{\mathrm{PP}}^2}$	-
θ_u	$\frac{2}{\rho(u^2+v^2)T_{\mathrm{m}}L_{\mathrm{PP}}^2}\left[mx_{\mathrm{G}}r-\frac{2u\left(M_z+I_z\dot{r}+m\left(x_{\mathrm{G}}(\dot{v}+ru)-y_{\mathrm{G}}(\dot{u}-rv)\right)\right)}{(u^2+v^2)}\right]$	-
$\theta_{\dot{u}}$	$\frac{-2my_{\mathrm{G}}}{\rho(u^2+v^2)T_{\mathrm{m}}L_{\mathrm{PP}}^2}$	-
θ_v	$\frac{2}{\rho(u^2+v^2)T_{\mathrm{m}}L_{\mathrm{PP}}^2}\left[my_{\mathrm{G}}r-\frac{2v\left(M_z+I_z\dot{r}+m\left(x_{\mathrm{G}}(\dot{v}+ru)-y_{\mathrm{G}}(\dot{u}-rv)\right)\right)}{(u^2+v^2)}\right]$	-
$\theta_{\dot{v}}$	$\frac{2mx_{\mathrm{G}}}{\rho(u^2+v^2)T_{\mathrm{m}}L_{\mathrm{PP}}^2}$	-
θ_r	$\frac{2m(x_{\mathrm{G}}u+y_{\mathrm{G}}v)}{\rho(u^2+v^2)T_{\mathrm{m}}L_{\mathrm{PP}}^2}$	-
$\theta_{\dot{r}}$	$\frac{2I_z}{\rho(u^2+v^2)T_{\mathrm{m}}L_{\mathrm{PP}}^2}$	-

Table 14 Definitions of the sensitivity coefficients for $U_{N'}$.

R	Var. (x)	L_{PP}	T_m	ρ	U_C	F
	Unit	m	m	kg/m^3	m/s	N,Nm
	Mag.	3.048	0.132	998.1	1.531	-
	B_x	0.002	0.001	0.041	0.011	-
X'	$\frac{\theta_x^2 B_x^2}{B_R^2}$ (%)	0.1	15.8	0.0	49.4	34.7
Y'		0.0	5.3	0.0	16.6	78.0
X'		0.1	3.2	0.0	10.1	86.6

F	$\frac{U_{F,x}^2}{U_F^2}$ (%)				U_F	$\lvert F\rvert$	$\frac{U_F}{\lvert F\rvert}$
	β	align	calib	acquis	[N]	[N]	(%)
F_x	91.8	1.7	0.0	6.5	0.122	10.9	1.1
F_y	97.0	1.8	0.0	1.2	0.826	28.5	2.9
M_z	96.8	1.8	0.1	1.4	1.118	44.1	2.5

R	U_R	$\frac{U_R^2}{U_R^2}$	U_R	$\frac{U_R^2}{U_R^2}$	U_R	$\lvert R\rvert$	$\frac{U_R}{\lvert R\rvert}$
	[10^{-2}]	(%)	[10^{-2}]	(%)	[10^{-2}]	[-]	(%)
X'	0.045	96.6	0.008	3.4	0.045	0.023	1.9
Y'	0.201	95.1	0.046	4.9	0.206	0.061	3.4
N'	0.085	94.5	0.020	5.5	0.087	0.031	2.8

Table 15 UA summary of static drift test (β = -10°).

R	Var. (x)	L_{PP}	T_m	x_G	y_G	m	I_z	ρ	u	v	r	$\dot{u}$	$\dot{v}$	$\dot{r}$	F
	Unit	m	m	m	m	kg	kgm^2	kg/m^3	m/s	m/s	rad/s	m/s^2	m/s^2	rad/s^2	N,Nm
	Mag.	3.048	0.132	-0.016	0.000	82.55	49.79	998.1	1.527	0.002	0.150	0.000	0.003	0.000	-
	B_x	0.002	0.001	0.005	0.002	0.11	1.84	0.041	0.010	0.006	0.003	0.002	0.002	0.000	-
X'	$\frac{\theta_x^2 B_x^2}{B_R^2}$ (%)	0.0	4.0	0.1	0.0	0.0	-	0.0	67.6	3.7	0.0	11.0	-	0.0	13.5
Y'		0.0	0.6	0.0	0.0	0.1	-	0.0	9.0	0.0	27.1	-	3.2	0.0	60.0
N'		0.0	8.1	3.3	0.0	0.0	0.0	0.0	24.8	0.0	0.0	0.0	0.0	0.0	63.5

F	r_{max}	$\frac{U_{F,x}^2}{U_F^2}$ (%)									U_F	F	$\frac{U_F}{\lvert F\rvert}$	D_F†	$\frac{U_F}{D_F}$
	[rad/s]	calib	acquis	u	v	r	$\dot{u}$	$\dot{v}$	$\dot{r}$	t	[N] [Nm]	[N] [Nm]	(%)	[N] [Nm]	(%)
F_x		0.0	4.3	11.5	0.0	4.0	55.1	25.0	0.0	0.1	0.140	-10.06	1.4	-	-
F_y	0.150	0.0	2.1	7.1	0.0	89.8	0.0	1.0	0.0	0.0	0.606	-27.27	2.2	4.36	1.1
M_z		0.4	2.0	0.8	0.0	95.8	0.1	0.9	0.0	0.0	0.457	-21.26	2.1	47.67	1.0

R	r_{max}	U_R	$\frac{U_R^2}{U_R^2}$	U_R	$\frac{U_R^2}{U_R^2}$	U_R	R	$\frac{U_R}{\lvert R\rvert}$	D_R†	$\frac{U_R}{D_R}$
	[rad/s]	[10^{-2}]	(%)	[10^{-2}]	(%)	[10^{-2}]	[-]	(%)	[-]	(%)
X'		0.081	24.7	0.142	75.3	0.163	-0.021	7.6	-	-
Y'	0.150	0.167	94.2	0.042	5.8	0.172	-0.017	10.0	0.034	5.0
N'		0.040	90.0	0.013	10.0	0.042	-0.015	2.8	0.031	1.4

† D: Dynamic range of the variable $D = |max - min|$

Table 16 UA summary of pure yaw test (r = r_{max}).

R	Var. (x)	L_{PP}	T_m	x_G	y_G	m	I_z	ρ	u	v	r	$\dot{u}$	$\dot{v}$	$\dot{r}$	F
	Unit	m	m	m	m	kg	kgm^2	kg/m^3	m/s	m/s	rad/s	m/s^2	m/s^2	rad/s^2	N,Nm
	Mag.	3.048	0.132	-0.016	0.000	82.55	49.79	998.1	1.518	0.269	0.000	0.000	0.001	-0.001	-
	B_x	0.002	0.001	0.005	0.002	0.11	1.84	0.041	0.010	0.008	0.000	0.000	0.000	0.000	-
X'	$\frac{\theta_x^2 B_x^2}{B_R^2}$	0.0	4.9	0.0	0.0	0.0	-	0.0	82.8	0.3	-	0.0	-	0.0	12.0
Y'		0.0	3.2	0.0	0.0	0.0	-	0.0	9.5	1.1	0.0	-	0.0	0.0	86.1
N'	(%)	0.1	3.5	0.0	0.0	0.0	0.0	0.0	10.5	0.2	0.0	0.0	0.0	0.5	85.2

F	v_{max}	$\frac{U_{F,x}^2}{U_F^2}$ (%)									U_F	F	$\frac{U_F}{\lvert F\rvert}$	D_F†	$\frac{U_F}{D_F}$
	[m/s]	calib	acquis	u	v	r	$\dot{u}$	$\dot{v}$	$\dot{r}$	t	[N] [Nm]	[N] [Nm]	(%)	[N] [Nm]	(%)
F_x		0.0	5.6	8.9	85.5	0.0	0.0	0.0	0.0	0.0	0.166	-13.91	1.2	-	-
F_y	0.269	0.0	0.7	0.0	99.2	0.0	0.0	0.1	0.0	0.0	1.168	-29.55	4.0	86.08	1.4
M_z		0.0	0.6	0.0	99.3	0.0	0.0	0.0	0.0	0.0	1.770	-47.10	3.8	94.46	1.9

R	v_{max}	U_R	$\frac{U_R^2}{U_R^2}$	U_R	$\frac{U_R^2}{U_R^2}$	U_R	R	$\frac{U_R}{\lvert R\rvert}$	D_R†	$\frac{U_R}{D_R}$
	[m/s]	[10^{-2}]	(%)	[10^{-2}]	(%)	[10^{-2}]	[-]	(%)	[-]	(%)
X'		0.100	35.4	0.135	64.6	0.168	-0.029	5.8	-	-
Y'	0.269	0.264	91.2	0.082	8.8	0.276	-0.062	4.5	0.133	2.1
N'		0.132	97.7	0.020	2.3	0.133	-0.032	4.1	0.065	2.1

† D: Dynamic range of the variable $D = |max - min|$

Table 17 UA summary of pure sway test (v = v_{max}).

R	Var. (x)	L_{PP}	T_m	x_G	y_G	m	I_z	ρ	u	v	r	$\dot{u}$	$\dot{v}$	$\dot{r}$	F
	Unit	m	m	m	m	kg	kgm^2	kg/m^3	m/s	m/s	rad/s	m/s^2	m/s^2	rad/s^2	N,Nm
	Mag.	3.048	0.132	-0.016	0.000	82.55	49.79	998.1	1.503	-0.263	0.151	0.001	0.004	0.000	-
	B_x	0.002	0.001	0.005	0.002	0.11	1.84	0.041	0.010	0.006	0.003	0.002	0.002	0.000	-
X'	$\frac{\theta_x^2 B_x^2}{B_R^2}$	0.0	3.8	0.0	0.0	0.0	-	0.0	60.2	1.5	2.2	8.8	-	0.0	23.5
Y'		0.0	2.8	0.0	0.0	0.1	-	0.0	2.6	0.5	16.1	-	2.0	0.0	76.0
N'	(%)	0.1	2.4	1.2	0.0	0.0	0.0	0.0	7.1	0.1	0.0	0.0	0.0	0.0	89.2

F	r_{max}	$\frac{U_{F,x}^2}{U_F^2}$ (%)									U_F	F	$\frac{U_F}{\lvert F\rvert}$	D_F†	$\frac{U_F}{D_F}$
	[rad/s]	calib	acquis	u	v	r	$\dot{u}$	$\dot{v}$	$\dot{r}$	t	[N] [Nm]	[N] [Nm]	(%)	[N] [Nm]	(%)
F_x		0.0	3.5	36.6	0.4	31.5	26.9	1.1	0.0	0.0	0.235	-15.78	1.5	-	-
F_y	0.151	0.0	0.0	13.3	36.7	45.8	0.3	3.9	0.0	0.0	0.872	2.94	29.7	67.48	1.3
M_z		0.1	0.4	1.8	53.0	38.5	0.2	5.9	0.1	0.0	0.896	19.54	4.6	66.37	1.4

R	r_{max}	U_R	$\frac{U_R^2}{R^2}$	U_C	$\frac{U_C^2}{R^2}$	R	R	$\frac{U_R}{\lvert R\rvert}$	D_R†	$\frac{U_R}{D_R}$
	[rad/s]	[10^{-2}]	(%)	[10^{-2}]	(%)	[10^{-2}]	[-]	(%)	[-]	(%)
X'		0.104	32.9	0.148	67.1	0.181	-0.027	6.8	-	-
Y'	0.151	0.214	82.4	0.099	17.6	0.236	0.047	5.0	0.065	3.6
N'		0.067	93.2	0.018	6.8	0.069	0.014	5.1	0.045	1.5

† D: Dynamic range of the variable $D = |max - min|$

Table 18 UA summary of yaw and drift test ($\boldsymbol{r} = \boldsymbol{r_{max}}$).

Appendix B.

Mean draft uncertainty $B_{T\mathrm{m}}$

If the model ship is ballasted based on displacement, U_{T_m} is composed of two uncorrelated elemental uncertainties, $U_{T_\mathrm{m},d1}$ from the model manufacturing and $U_{T_\mathrm{m},d2}$ from the uncertainty related to ballast weights. By assuming the model uncertainty to be ±1mm in all coordinates, as given in ITTC Procedure 7.5-01-01-01 Rev 01, 'Ship Models', and these dimensions are changed while keeping the block coefficient constant, the uncertainty in the displacement of the model can be calculated using

$$\nabla' = \rho(L+\varepsilon_L)(B+\varepsilon_B)(T+\varepsilon_T) \qquad \text{(A1)}$$

where, ρ is the water density, L, B, T are model length, beam, draft, respectively, and ε_L=2mm, ε_B=2mm, ε_T=1mm are uncertainties in length, beam, draft, respectively. Then $U_{T_\mathrm{m},d1}$ can be estimated as

$$U_{T_\mathrm{m},d1} = \frac{\nabla' - \nabla}{\rho A_{WP}} = 0.0011\mathrm{m} \qquad \text{(A2)}$$

where A_{WP} is the water plane area of the model given in Table 1. $U_{T_\mathrm{m},d2}$ can be estimated from the total mass bias U_m by equating with the displacement change

$$U_{T_\mathrm{m},d2} = \frac{U_m}{\rho A_{\mathrm{WP}}} = 0.0001\mathrm{m} \qquad \text{(A3)}$$

Then, U_{T_m} = 0.001m is estimated as the RSS of $U_{T_\mathrm{m},d1}$ and $U_{T_\mathrm{m},d2}$.

Appendix C.

Moment of inertia uncertainty U_{Iz}.

Generally, yaw moment of inertia can be measured by measuring yawing periods T while swinging a given mass attached to, for example, a steel rod with known torsion stiffness G (*swinging method*), or by measuring the yaw moment while enforcing a sinusoidal yaw motion to the mass (*yawing method*).

If the *swinging method* is used, the moment of inertia of the mass is

$$I_z = GgT^2 \qquad \text{(C1)}$$

where g is the gravitational acceleration. The uncertainty of the measured I_z can be estimated as:

$$U_{I_z}^2 = \theta_G^2 U_G^2 + \theta_T^2 U_T^2 \qquad \text{(C2}$$

where, sensitivity coefficients are calculated by differentiating equation (C1) with respect to each variable. The uncertainties U_G and U_T should be estimated according to their test procedures used. Details of this method are provided in by Simonsen C. (2004).

If the *yawing method* is used, the moment of inertia of the mass is determined from the motion equation of simple yaw:

$$-M_z = I_z\ddot{\psi}$$

where, $\psi = -\psi_o \cos\omega t$ and M_z is the moment measured during the applied yaw motion. By expanding the measured moment with the Fourier series with the applied yaw motion frequency ω as the base frequency,

$$I_z = \frac{M_Z^{FSC1}}{\psi_0 \omega^2} \qquad \text{(C3)}$$

where, M_z^{FSC1} is the 1st harmonic amplitude of measured yaw moment, ψ_0 is the applied yaw motion amplitude, and $\omega = 2\pi \mathrm{N}/60$ is the yaw motion frequency.

$$M_z^{FSC1} = \frac{2}{J}\sum_{j=1}^{J} M_{z\,j} \cos \omega t_j \qquad \text{(C4)}$$

If multiple measurements with combinations of different ψ_0's and ω's are conducted, the yaw moment of inertia can be determined with a least-square (LS) regression method.

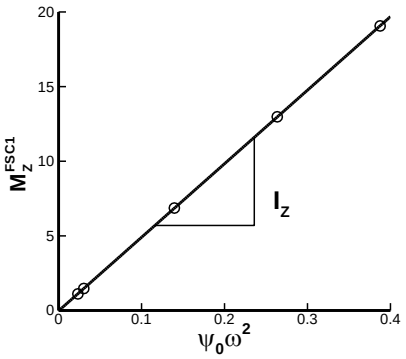

Hence the uncertainty of the measured yaw moment of inertia U_{I_z} is considered as the RSS of each uncertainty of individual measurement $U_{I_z,i}$ and the uncertainty related to least squaring which is $U_{I_z,LS}$:

$$U_{I_z}^2 = \sum_i U_{I_z,i}^2 + U_{I_z,LS}^2 \qquad \text{(C5)}$$

$U_{I_z,i}$ in equation (C5) can be defined as

$$U_{I_z,i}^2 = \theta_{M_{z,i}^{FSC1}}^2 U_{M_{z,i}^{FSC1}}^2 + \theta_{\psi_0,i}^2 U_{\psi_0,i}^2 + \theta_{\omega,i}^2 U_{\omega,i}^2 \qquad \text{(C6)}$$

Sensitivity coefficients are calculated analytically from the equation (C5). $U_{M_{z,i}^{FSC1}}$ is defined from equation (C4),

$$U_{M_{z,i}^{FSC1}}^2 = \sum_{j=1}^{J} \theta_{M_{z,i_j}}^2 U_{M_{z,i_j}}^2 + \theta_{\omega_i}^2 U_{\omega_i}^2 + \sum_{j=1}^{J} \theta_{t_j}^2 U_{t_j}^2 \qquad \text{(C7)}$$

where, $U_{\omega_i} = 2\pi U_{\mathrm{N}}/60$. $U_{M_{z\,j}}$ is estimated as 3% of $U_{M_z^{FSC1}}$. Finally $U_{I_z,LS}$ is quantified with the standard estimate of error (SEE) from Coleman and Steel (1999),

$$U_{I_z,LS} = \sqrt{\sum_{i=1}^{L} \frac{\left(I_z - I_{z,i}\right)^2}{L-1}} \qquad \text{(C8)}$$

where, I_z is the least squared regression result and $I_{z,i}$ is the result of individual measurements.

If the yaw moment of inertia of the model ship is measured together with a mount or a yoke to hold the model ship, and if part of ballasting weights is added or removed while mounting, the yaw moment of inertia of the model is

$$I_z = I_{z,\mathrm{Total}} - I_{z,\mathrm{mount}} \pm \sum_k I_{z,\mathrm{ballast},k} \qquad \text{(B9)}$$

where, I_z is the moment of inertia of the model, $I_{z,\mathrm{Total}}$ is the total moment of inertia of combined model and mount or yoke, $I_{z,\mathrm{mount}}$ is that of the mount or yoke, and $I_{z,\mathrm{ballast},k}$ is the moment of inertia of the ballast weights added or excluded. If the moment of inertia of each ballast weight with respect to its own axis and the distance to the mid ship are known, the moment of inertia of the ballast weight is calculated by using the parallel axis theorem

$$\sum_k I_{z,\mathrm{ballast},k} = \sum_k \left(I_{z,\mathrm{own},k} + r_k^2 m_k\right) \qquad \text{C10)}$$

where r_k is the distance to the mid ship and m_k is the weight of the ballast weight. By applying the uncertainty propagation equation to equation (C10), $U_{I_z,\mathrm{ballast},k}$ is

$$U_{I_z,\mathrm{ballast},k}^2 = \theta_{I_z,\mathrm{own},k}^2 U_{I_z,\mathrm{own},k}^2 + \theta_{r_k}^2 U_{r_k}^2 + \theta_{m_k}^2 U_{m_k}^2 \qquad \text{(C11)}$$

Then U_{I_z} is

$$U_{I_z}^2 = U_{I_z,\text{Total}}^2 + U_{I_z,\text{mount}}^2 + \sum_k U_{I_z,\text{ballast},k}^2 \quad \text{(C12)}$$

$U_{I_z,\text{Total}}$ and $U_{I_z,\text{mount}}$ can be estimated either from equation (C1) or (C5) according to I_z measurement method used, and $U_{I_z,\text{ballast},k}$ can be estimated from equation (C10), respectively.

An example with yawing method is presented in Table B.

	i	ψ_0	f	$M_{z,i}^{FSC1}$	$I_{z,i}$	$\theta_{M_{z,i}^{FSC1}}^2 U_{M_{z,i}^{FSC1}}^2$	$\theta_{\psi_0,i}^2 U_{\psi_0,i}^2$	$\theta_{\omega,i}^2 U_{\omega,i}^2$	$U_{I_z,i}$	$I_z - I_{z,i}$
		[deg]	[Hz]	[Nm]	[kgm^2]	[kgm^2]	[kgm^2]	[kgm^2]	[kgm^2]	[kgm^2]
Model + Mount	1	9.0	0.15	6.86	49.19	1.01E-03	1.45E+00	4.30E-05	1.20	5.16E-02
	2	17.0	0.15	12.98	49.24	1.31E-02	4.06E-01	4.31E-05	0.65	2.69E-03
	3	9.0	0.25	19.07	49.19	7.07E-02	1.45E+00	1.55E-05	1.23	5.05E-02
	$U_{I_z}^2 = \sum_i^L U_{I_z,i}^2 + \left(2\sqrt{\sum_i^L \frac{(I_z - I_{z,i})^2}{L-2}}\right)^2$; $I_{z,\text{Total}}$=49.19kgm^2 , $U_{I_{z,\text{Total}}}$= 1.84kgm^2									
Mount	1	9.0	0.15	0.15	1.05	7.67E-10	6.61E-04	1.97E-08	0.03	4.89E-02
	2	17.0	0.15	0.28	1.08	5.89E-09	1.95E-04	2.07E-08	0.01	2.23E-02
	3	9.0	0.25	0.42	1.08	1.92E-08	7.01E-04	7.51E-09	0.03	1.76E-02
	$I_{z,\text{mount}}$=1.10 kgm^2 , $U_{I_{z,\text{mount}}}$= 0.12 kgm^2									
	k	Item	$I_{z,\text{own},k}$ [kgm^2]	$\varepsilon_{I_{z,\text{own},k}}$ [kgm^2]	m_k [kg]	ε_{m_k} [kg]	r_k [m]	ε_{r_k} [m]	$U_{I_{z,\text{own},k}}$ [kgm^2]	
Ballast Weights	1	Part 1	0.0014	0.00006	1.109	0.02	0.0	0.001	0.00006	
	2	Part 2	0.0014	0.00006	1.109	0.02	0.75	0.001	0.01137	
	3	Part 3	0.0014	0.00006	1.109	0.02	0.75	0.001	0.01137	
	4	weight 1	0.0257	0.00047	2.285	0.04	0.118	0.001	0.00091	
	5	weights 6, 11, 12, 13	0.0726	0.00080	9.122	0.08	0.211	0.001	0.00531	
	$I_{z,\text{ballast}} = \sum_k (I_{z,\text{own},k} + r_k^2 m_k)$ $U_{I_{z,\text{ballast}}}^2 = \sum_k U_{I_{z,\text{ballast},k}}^2$, $U_{I_{z,\text{ballast},k}}^2 = \theta_{I_{z,\text{own},k}}^2 U_{I_{z,\text{own},k}}^2 + \theta_{r_k}^2 \varepsilon_{r_k}^2 + \theta_{m_k}^2 \varepsilon_{m_k}^2$ $I_{z,\text{ballast}}$=1.70kgm^2 , $U_{I_{z,\text{ballast}}}$= 0.017kgm^2									
Model	$I_z = I_{z,\text{Total}} - I_{z,\text{mount}} + I_{z,\text{ballast}}$= 49.79kgm^2 $U_{I_z} = \sqrt{U_{I_z}^2 + U_{I_{z,\text{mount}}}^2 + U_{I_{z,\text{ballast}}}^2}$= 1.84kgm^2									

Table B. Moment of inertia uncertainty U_{I_z} estimation.

Appendix D.

Carriage speed uncertainty U_{Uc}.

Carriage speed bias limit U_{U_C} is estimated end-to-end by calibrating the carriage speed with respect to reference speeds. Reference speeds are obtained by measuring travel time Δt for a known distance ΔL.

$$U_{\text{ref}} = \frac{\Delta L}{\Delta t} \quad \text{(D1)}$$

U_{U_C} is composed of two uncorrelated elemental uncertainties; the calibration uncertainty $U_{U_C,\text{calib}}$ and the data-acquisition uncertainty $U_{U_C,\text{acquis}}$,

$$U_{U_C}^2 = U_{U_C,\text{calib}}^2 + U_{U_C,\text{acquis}}^2 \quad \text{(D2)}$$

where, $U_{U_C,\text{calib}}$ is the RSS of the individual reference speed calibrations,

$$U_{U_{C,calib}} = \sqrt{\sum_i \left(\theta_{\Delta L_i}^2 U_{\Delta L_i}^2 + \theta_{\Delta t_i}^2 U_{\Delta t_i}^2\right)^2} \quad \text{(C3)}$$

where, $U_{\Delta L}$ and $U_{\Delta t}$ are the uncertainties of ΔL and Δt, respectively. $U_{U_C,\text{acquis}}$ is quantified with the standard estimate of error (SEE) as per ITTC guidelines

$$U_{U_C,\text{acquis}} = 2SEE = 2\sqrt{\sum_i^N \frac{\left(U_{C,i} - U_{\text{ref},i}\right)^2}{N-2}} \quad \text{(D4)}$$

The carriage speed measurement results are summarized in Table C.

i	ΔL_i [m]	Δt_i [s]	$U_{\text{ref},i}$ [m/s]	$U_{C,i}$ [m/s]	$U_{U_C,\text{calib},i}$ [m/s]
1	24.088	30.6301	0.7864	0.7840	0.000163
2	24.088	30.6985	0.7847	0.7823	0.000163
3	24.088	30.7130	0.7843	0.7816	0.000163
4	14.989	11.5026	1.5639	1.5601	0.000435
5	14.989	11.5102	1.5629	1.5590	0.000435
6	14.989	11.5204	1.5615	1.5576	0.000434
7	14.989	4.9269	2.2694	2.2631	0.000631
8	14.989	4.9315	2.2681	2.2619	0.000631
9	14.989	4.9273	2.2693	2.2629	0.000631

$U_{\Delta L}$=0.005m, $U_{\Delta t}$=0.0001sec

$U_{U_C,\text{calib}} = \sqrt{\sum_i \left(\theta_{\Delta L_i}^2 U_{\Delta L_i}^2 + \theta_{\Delta t_i}^2 U_{\Delta t_i}^2\right)^2}$ = 0.0014m/s

$U_{U_C,\text{acquis}} = 2\sqrt{\sum_i^N \frac{\left(U_{C,i} - U_{\text{ref},i}\right)^2}{N-2}}$ = 0.0102m/s

$U_{U_C} = \sqrt{U_{U_C,\text{calib}}^2 + U_{U_C,\text{acquis}}^2}$ = 0.0102m/s

Table C. Carriage speed uncertainty UB_{U_C}. used in this example

Appendix E.

Drift angle uncertainty U_β.

The uncertainty of the drift angle U_β is composed of two uncorrelated uncertainties $U_{\beta,\text{align}}$ and $U_{\beta,\text{drift}}$.

$$\boldsymbol{U_\beta = \sqrt{U^2_{\beta,\text{align}} + U^2_{\beta,\text{drift}}}} \qquad \text{(E1)}$$

$U_{\beta,\text{align}}$ is the model installation uncertainty with respect to straight towing direction and assumed to be 0.03°.

$U_{\beta,\text{drift}}$ is the deviation from the drift angle setting and it is estimated end-to-end by calibrating the drift angle with respect to reference angles. Reference angle is achieved by measuring the chord length of the arc swept by a fixed position on the model ship due to drift angle setting.

$$\beta_{\text{ref}} = \cos^{-1}\left(1 - \frac{C^2}{2R^2}\right) \qquad \text{(E2)}$$

The concept of reference angle measurement is illustrated as

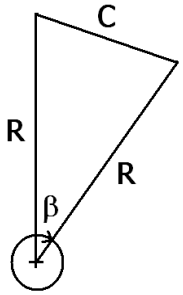

where, C is the chord length measured, R is the distance between mid ship and the measurement position. Then $U_{\beta,\text{drift}}$ can be further decomposed into two uncorrelated uncertainties $U_{\beta,\text{calib}}$ and $U_{\beta,\text{acquis}}$. The procedure to estimate these uncertainties is similar with U_{U_C} estimation. $U_{\beta,\text{drift}}$ measurement results are summarized in Table D. Finally, B_β=0.22° is estimated from the RSS of $U_{\beta,\text{align}}$ and $U_{\beta,\text{drift}}$.

i	R_i [m]	C_i [m]	$\beta_{\text{ref},i}$ [deg]	β_i [deg]	$U_{\beta,\text{calib},i}$ [deg]
1	1.998	0.068	1.96	2.00	0.00050
2	1.998	0.137	3.94	4.00	0.00050
3	1.998	0.207	5.94	6.00	0.00050
4	1.998	0.276	4.93	8.00	0.00050
5	1.998	0.344	9.87	10.00	0.00050
6	1.998	0.414	11.88	12.00	0.00051
7	1.998	-0.067	-1.93	-2.00	0.00050
8	1.998	-0.137	-3.92	-4.00	0.00050
9	1.998	-0.206	-5.92	-6.00	0.00050
10	1.998	-0.275	-4.88	-8.00	0.00050
11	1.998	-0.343	-9.84	-10.00	0.00050
12	1.998	-0.413	-11.86	-12.00	0.00051

$\beta_{\text{ref},i} = \cos^{-1}\left(1 - \frac{C^2}{2R^2}\right)$; ε_R=ε_C=0.001m

$U_{\beta,\text{calib},i} = \sqrt{\theta^2_{R_i}\varepsilon^2_R + \theta^2_{C_i}\varepsilon^2_C}$

$U_{\beta,\text{calib}} = \sqrt{\sum_i U^2_{\beta,\text{calib},i}} = 0.002°$

$U_{\beta,\text{acquis}} = 2\sqrt{\sum_i^N \frac{(\beta_i - \beta_{\text{ref},i})^2}{N-2}} = 0.222°$

$U_{\beta,\text{drift}} = \sqrt{U^2_{\beta,\text{calib}} + U^2_{\beta,\text{acquis}}} = 0.222°$

Table D. Uncertainty in the drift angle U_β.